Available online at www.sciencedirect.com
ScienceDirect
Journal of Organometallic Chemistry 693 (2008) 947–956
Journal of Organometallic Chemistry
www.elsevier.com/locate/jorganchem

Theoretical studies on structures and spectroscopic properties of bis-cyclometalated iridium complexes $[Ir(ppy)_2X_2]^-$

Tao Liu [a], Hong-Xing Zhang [a,*], Bao-Hui Xia [a,b]

[a] State Key Laboratory of Theoretical and Computational Chemistry, Institute of Theoretical Chemistry, Jilin University, Changchun 130023, People's Republic of China
[b] College of Chemistry, Jilin University, Changchun 130023, People's Republic of China

Received 20 September 2007; received in revised form 30 November 2007; accepted 5 December 2007
Available online 15 December 2007

Abstract

The electronic structures and spectroscopic properties of a series of mixed bis-cyclometalated iridium(III) complexes $[Ir(ppy)_2X_2]^-$ (X = CN, **1**; X = NCS, **2**; X = NCO, **3**; ppy = 2-phenylpyridl) were investigated at the B3LYP/LANL2DZ and CIS/LANL2DZ levels. The calculated geometry parameters in the ground state are well consistent with the corresponding experimental values. The HOMO of **1** is dominantly localized on Ir atom and ppy ligand, but the HOMO of **2** and **3** have significant X ligand composition. Under the TD-DFT level with PCM model, the absorption and phosphorescence in CH_2Cl_2 media were calculated based on the optimized geometries in the ground and excited states, respectively. The lowest-lying absorption of **1** at 403 nm is attributed to $\{[d_{x^2-y^2}(Ir)+ d_{xy}(Ir) + \pi(ppy)] \rightarrow [\pi^*(ppy)]\}$ transition with metal-to-ligand and intraligand charge transfer (MLCT/ILCT) transition characters, whereas those of **2** (449 nm) and **3** (475 nm) are related to $\{[d_{x^2-y^2}(Ir) + d_{xy}(Ir) + \pi(ppy) + \pi(NCS/NCO)] \rightarrow [\pi^*(ppy)]\}$ transition with MLCT/ILCT and ligand-to-ligand charge transfer (LLCT) transition characters. The phosphorescence of **1** at 466 nm can be described as originating from $^3\{[d_{x^2-y^2}(Ir) + d_{xy}(Ir) + \pi(ppy)][\pi^*(ppy)]\}$ excited state, while those of **2** (487 nm) and **3** (516 nm) originate from $^3\{[d_{x^2-y^2}(Ir) + d_{xy}(Ir) + \pi(ppy) + \pi(NCS/NCO)][\pi^*(ppy)]\}$ excited states. The calculated results showed that the transition character of the absorption and emission can be changed by adjusting the π electron-accepting abilities of the X ligands and the phosphorescent color can be tuned by altering the X ligands.

Keywords: Iridium complexes; Luminescence; Excited state; B3LYP; CIS

1. Introduction

Organometallic complexes with d^6 electronic configuration such as Os(II), Ir(III), Ru(II), and Re(I) have attracted much attention [1–4], due to that they played an important roles as highly efficient electroluminescent (EL) emitters in fields related to organic light emitting devices (OLEDs) [5], biological labeling reagents [6], photocatalysts for CO_2 reduction [7], and sensors [8]. In principle, the phosphorescence originated from the triplet state is spin-forbidden, but it can be achieved through the spin–orbit coupling of the heavy metal, and their long-lived triplet state emissions with high luminescent efficiencies can increase the likelihood of either energy or electron transfer occurring before radiative or nonradiative relaxation, and the singlet and triplet metal-to-ligand charge transfer (MLCT) transitions can be mixed together, which results in that the ^{3}MLCT state can emit effectively by borrowing the intensity of singlet MLCT state. Thus, in theory, internal phosphorescence quantum efficiency can achieve as high as 100% [9]. Among these heavy metal complexes, Ir(III) complexes are the most effective and tunable phosphorescent material, in addition, they are more sublimable than other metal complexes, which is the most advantageous for device fabrication [10].

Since it was reported that OLEDs fabricated by tris-cyclometalated complexes such as fac-$[Ir(ppy)_3]$

* Corresponding author. Tel.: +86 431 8498966; fax: +86 431 8945942.
E-mail address: zhanghx@mail.jlu.edu.cn (H.-X. Zhang).

0022-328X/$ - see front matter © 2008 Elsevier B.V. All rights reserved.
doi:10.1016/j.jorganchem.2007.12.014

($ppy^- = 2$-phenylpyridine) has efficiencies greater than 80%, Ir(III) complexes have devoted to considerable much attention [11–14]. Numerous bis- and tris-cyclometalated Ir complexes such as $Ir(C^\wedge N)_3$ and $Ir(C^\wedge N)_2L$ types have been synthesized and investigated by Thompson [11,15] and Hay [13] experimentally and theoretically. Both of them came to a similar conclusion that the phosphorescence predominantly originate from $^3(\pi\pi^*)$ and ^{3}MLCT excited states, and the phosphorescent color can be adjusted from green to red by changing C^N ligands. On application, Thompson and Forrest have successfully fabricated lots of red and blue OLEDs with various Ir complexes bearing simple ppy derivatives ligand such as bzq, btp, and fppy, and these OLEDs have excellent quantum efficiency [16]. Furthermore, Wong et al. [10] introduced fluorene derivatives as C^N ligand into Ir complexes, these new fluorene C^N ligand with electron-donating diphenylamino groups can increase the energy level of the HOMO, and add hole-transporting ability to the phosphorescent center. So the OLEDs fabricated by this kind of Ir complexes as phosphorescent dopant emitters show very high efficiencies.

Previous theoretical investigations showed that the HOMO is dominantly composed of d(Ir) and π(ligand), and the LUMO is localized on ligands, so the lowest-lying absorption is always assigned to two types of metal-to-ligand charge transfers (MLCT/ML′CT) transition, and other absorption transitions are attributed to MLCT, ligand-to-ligand charge transfer (LLCT), inter-ligand charge transfer (ILCT), and mixing transitions of MLCT/LLCT/ILCT. Furthermore, the theoretical work proved that the emission color can be tuned by changing HOMO–LUMO gap and helped to design new luminescent Ir complexes with high efficiency [13,17–19].

Recently, a new series of Ir complexes TBA[$Ir(ppy)_2(X)_2$] (X = CN, NCS, and NCO; ppy = 2-phenylpyridl; TAB = tetrabutylammonium cation) have been synthesized and investigated by Nazeeruddin [20] and co-workers experimentally. These complexes exhibit unprecedented phosphorescence quantum yields of $97 \pm 3\%$ with an excited-state lifetimes of 1–3 μs in dichloromethane solution. But the theoretical study on the spectral properties of these complexes from an electronic structure point of view and the relationship between X ligand and the spectra is sparse.

We carried out the present work, aimed at providing an in-depth theoretical understanding of the structures and spectroscopic properties of Ir(III) cyclometalated complexes as well as the relationship between the spectra and the X ligands. Herein, we performed theoretical calculation on $[Ir(ppy)_2X_2]^-$ (X = CN, **1**; X = NCS, **2**; X = NCO, **3**) in the ground and excited states using ab initio and density functional theory (DFT) methods. Highly important, the effects of the peripheral X ligands on the phosphorescence have been revealed so that the phosphorescent color can be tuned by adjusting X ligands.

2. Computational details and theory

The ground state geometries were fully optimized by DFT [21] method with Becke's three parameter functional and the Lee–Yang–Parr functional [22] (B3LYP). On the basis of the optimized geometries in the ground state, the absorption in dichloromethane (CH_2Cl_2) media were calculated by time-dependent DFT (TDDFT) [23] associated with the polarized continuum model (PCM) [24].

Configuration interaction singles (CIS) [25,26] method, presenting a general zeroth-order treatment to excited state just as HF for the ground state of molecular systems, is successful in the structure optimization of the excited state proved by many researcher [19,27]. The wave function, energy, and analytic gradient of a molecule in an electronic excited state are available for the CIS method [26,28,29]. However, the transition energies obtained by the CIS calculations are usually overestimated since the CIS method uses the orbitals of a HF state in an ordinary CI procedure to solve for the higher roots and only considered parts of the electronic correlation effects via the mixing of excited determinants [28,29]. In our work, we rectify the excited state properties by time-dependent DFT (TD-DFT) method to compensate the flaw of the CIS method. This kind of theoretical approach has been proven to be reliable for transition-metal complex systems [19,27].

In the calculations, the quasi-relativistic pseudo-potentials of Ir atoms proposed by Hay and Wadt [30] with 17 valence electrons were employed, and the LANL2DZ basis sets were adopted. The basis sets were described as Ir [8s6p3d]/[3s3p2d], C, N, O, and S [10s5p]/[3s2p], and H [4s]/[2s]. Thus, 306 basis functions and 206 electrons for **1**, 322 basis functions and 218 electrons for **2**, and 324 basis functions and 222 electrons for **3** were included in the calculations. All of the calculations were accomplished by using the GAUSSIAN 03 software package [31] on an Origin/3900 server.

The optimized ground and excited states geometries display C_2 symmetry. As shown in Fig. 1, the x/C_2 axis is oriented through Ir atom and the center of two X ligands, the z and y axes both deviate 45° from the plane defined by two X ligands. Two ppy ligands are almost perpendicular to each other. Under the C_2 symmetry and the basis sets employed, the total 306 orbitals of **1** are reduced to 154a and 152b irreducible orbitals, while the total 322 orbitals of **2** are reduced to 162a and 160b irreducible orbitals, likewise, the 324 orbitals of **3** are reduced to 163a and 161b irreducible orbitals. All these orbitals are included in the DFT calculations in order to have all of the possible electron correlations in the present computational level.

3. Results and discussion

3.1. The ground and the excited states geometries

The main optimized geometry structural parameters in the ground state together with the X-ray crystal diffraction

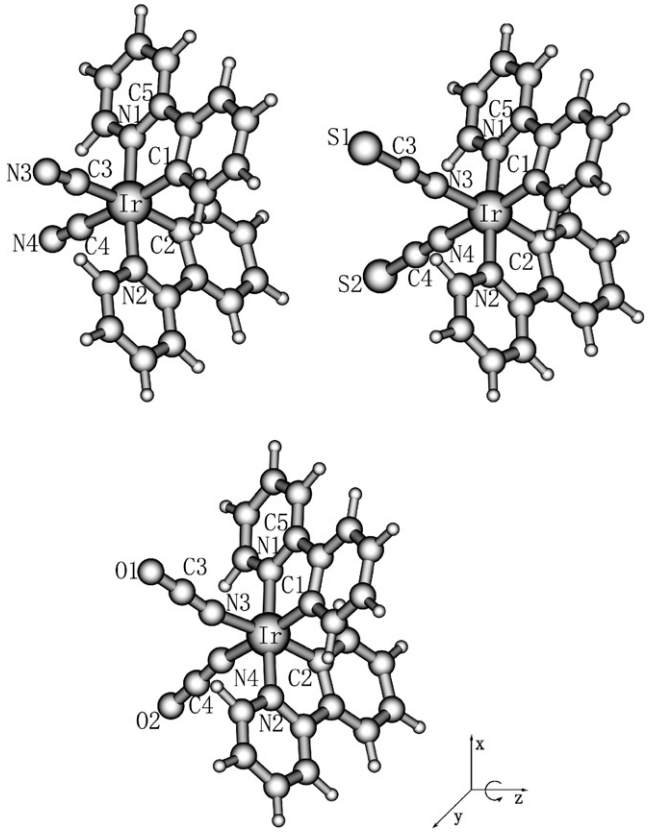

Fig. 1. Optimized geometry structures of **1**–**3** at the B3LYP/LANL2DZ level.

data of $Ir(ppy)_2acac$ [11] are given in Table 1, and the optimized geometries are shown in Fig. 1. Because our attempts to optimize the molecular geometry in solvents failed (this experience is similar to that of De Angelis et al. [2b]), we used the geometries obtained in the gas phase for all spectrum calculations. The vibration frequencies of **1**–**3** were calculated based on the optimized geometries to verify that each of the ground state geometries is a minimum (no minus frequency) on the potential energy surface. The calculated results revealed that all of the complexes have X^1A ground state. Two ppy ligands are almost perpendicular to each other because C(5)–N(1)–Ir–C(2) dihedral angle is close to 90°. Furthermore, the optimized bond lengths and bond angles of **1**–**3** in the ground state are in general agreement with the corresponding experimental values of $Ir(ppy)_2acac$. Take **2** for example, the calculated bond lengths of Ir–N(1)/N(2) (2.057 Å) and Ir–C(1)/C(2) (2.022 Å) are overestimated by ca. 0.046 Å and 0.018 Å in comparison with the measured values. Table 1 shows that the N(1)–Ir–N(2) bond angle of **1** (174.3°) is smaller than those of **2** (176.1°) and **3** (176.6°), which due to that CN ligand is smaller than NCS/NCO ligands, so the force between CN ligand and $Ir(ppy)_2$ fragments is weaker than those between NCS/NCO ligand and $Ir(ppy)_2$ fragments. Table 1 shows that C(3)–N(3)–Ir of **2** (176.5°) is larger than that of **3** (166.4°), which due to the S=C group is larger that O=C group, so the repulsion between two X ligand of **2** is larger than that of **3**.

The main geometry structural parameters of **1**–**3** in A^3B excited states are given in Table 1. The calculated results showed that the bond lengths, bond angles, and dihedral angles are slightly changed relative to those in the ground state and the three complexes show similar variation trends. The calculated Ir–C(1)/C(2), Ir–C(3) and Ir-N(1)/N(2) bond lengths relax by 0.03 Å, but the C(3)≡N(3) and N(3)=C(3) bond lengths are strengthened by about

Table 1
Main optimized geometry structural parameters of the complexes in the ground and the lowest lying triplet excited state at the B3LYP and CIS level, respectively, together with the experimental values of $Ir(ppy)_2acac$

	1		**2**		**3**		$Ir(ppy)_2acac$
	X^1A	A^3B	X^1A	A^3B	X^1A	A^3B	Expt.[a]
Bond lengths (Å)							
Ir–N(1)	2.062	2.093	2.057	2.088	2.050	2.085	2.010(9)
Ir–C(1)	2.065	2.080	2.022	2.048	2.019	2.050	2.003(9)
Ir–C(3′)	2.077	2.111					
Ir–N(3)			2.138	2.140	2.145	2.141	
C(3)≡N(3)/N(3)=C(3)	1.193	1.167	1.192	1.159	1.202	1.172	
C(3)–S(1)/O(1)			1.688	1.706	1.242	1.226	
Bond angles (°)							
C(3)–Ir–C(4)	91.0	91.0					
C(1)–Ir–C(2)	90.0	89.2	90.5	89.8	91.1	90.3	
N(1)–Ir–N(2)	174.3	174.0	176.1	175.9	176.6	176.2	176.3(4)
N(3)–Ir–N(4)			89.4	89.8	89.0	89.7	
N(3)–C(3)–Ir	178.0	178.0					
C(3)–N(3)–Ir			176.5	177.0	166.4	171.7	
N(1)–Ir–C(1)	79.7	79.7	80.5	80.2	80.5	80.2	81.7(4)
Dihedral angles (°)							
C(5)–N(1)–Ir–C(2)	93.6	93.6	92.1	93.1	91.4	92.6	

[a] From Ref. [11].

Table 2
Molecular orbital compositions (%) in the ground state for $Ir(ppy)_2(CN)_2$ (**1**) at B3LYP level

Orbital	Energy (eV)	MO composition			Main bond type	Ir component
		Ir	ppy	CN		
54a	−0.7040	1.3	98.5	0.2	π^*(ppy)	
53b	−0.8237	1.6	98.3	0.1	π^*(ppy)	
53a	−1.2207	3.6	95.4	1.0	π^*(ppy)	
52b	−1.2716	2.1	96.7	1.2	π^*(ppy)	
HOMO–LUMO energy gap						
52a	−5.0790	47.4	45.9	6.7	d(Ir) + π(ppy)	34.0 $d_{x^2-y^2}$, 11.6 d_{xy}
51b	−5.6521	51.1	42.3	6.6	d(Ir) + π(ppy)	41.1 d_{yz}, 9.5 d_{xz}
51a	−5.6728	59.5	31.1	9.4	d(Ir) + π(ppy)	25.6 d_{xy}, 32.4 d_{z^2}
50b	−5.7441	15.8	76.2	8.0	d(Ir) + π(ppy)	10.1 d_{yz}

0.03 Å, which indicates that the ppy and X ligands have a trend to break away from Ir atom and the X ligands becomes more compact in the excited state than that in the ground state. The calculated bridging C–C bond of phenyl and pyridyl is shorted 0.02 Å in the triplet excited states relative to these in the ground states, which is consistent with the conclusion obtained by De Angelis et al. [2b]. The calculated N(3)–Ir–N(4) bond angle of **2** and **3** are increased by 0.4° and 0.7°, while the C(5)–N(1)–Ir–C(2) dihedral angle keeps close to 90°, which indicates that the two X ligands have a trends to break away from each other and the two ppy ligands maintain a right-angle in the excited state. The slight changes of the geometry structural parameters result from the electron transfer from the Ir–X bonding orbital to the π^*(ppy) orbital (vide infra) upon excitation, so the energies of Ir–X and Ir–ppy bonds are reduced.

The calculated stretching frequencies of ν(C≡N) and ν(N=C) of **1**–**3** in the ground state are consistent with the experimental results and the variations of the stretching frequencies between the ground and excited states agree well with the differences of the ground and excited state geometry parameters. Firstly, the calculated ν(C≡N) and ν(N=C) stretching frequency at 2117 cm^{-1}, 2139 cm^{-1} and 2256 cm^{-1} of **1**, **2**, and **3**, respectively, in ground state are agree well with the experimental results [20] at 2092 cm^{-1}, 2099 cm^{-1} and 2229 cm^{-1}. Secondly, the ν(C≡N) stretching frequency of **1** appears at 2117 $cm^{-1}$and 2125 cm^{-1} in the ground and excited states, respectively. The increase of the C≡N stretching frequency in the excited state indicates the stronger bonding interaction, which is consistent with shorten of the C≡N bond length in the excited state. The variations of the ν(N=C) stretching frequency of **2** and **3** are similar to the case for ν(C≡N). Similar vibration characteristics have also been found for $[OsN(C{\equiv}CH)_4]$ [33], the Os≡N bond is lengthened in the excited state compared to that in ground state, which is in agreement with the lower vibration frequency of ν(Os–N) (∼780 cm^{-1}) in the excited state as compared to that (∼1175 cm^{-1}) in the ground state.

3.2. The frontier molecular orbital properties

The frontier molecular orbital compositions (population analysis using the SCF density) of **1**–**3** are given in Tables 2–4. Tables 2–4 show that low unoccupied MOs dominantly localized on π^*(ppy) with more than 95.0% composition are hardly affected by X ligand, and the energy levels of LUMO and LUMO + 1 are very close. In contrast, the compositions of occupied MOs are dramatically changed by altering X ligands. For **1**, the highest occupied molecule orbital (HOMO) 52a, lying −5.079 eV, is dominantly com-

Table 3
Molecular orbital compositions (%) in the ground state for $Ir(ppy)_2(NCS)_2$ (**2**) at B3LYP level

Orbital	Energy (eV)	MO composition			Main bond type	Ir component
		Ir	ppy	NCS		
56b	−0.9170	1.5	98.0	0.5	π^*(ppy)	
56a	−1.3342	3.9	94.9	1.2	π^*(ppy)	
55b	−1.3935	2.5	96.1	1.4	π^*(ppy)	
HOMO–LUMO energy gap						
55a	−4.8801	46.3	29.2	24.5	d(Ir) + π(ppy) + π(NCS)	32.3 $d_{x^2-y^2}$, 12.5 d_{xy}
54b	−5.3591	38.6	13.2	48.2	d(Ir) + π(ppy) + π(NCS)	13.7 d_{yz}, 24.9 d_{xz}
54a	−5.3721	36.9	11.3	51.8	d(Ir) + π(ppy) + π(NCS)	35.4 d_{z^2}
53b	−5.6480	0.1	14.6	85.3	π(ppy) + π(NCS)	
53a	−5.8347	1.9	39.9	58.2	π(ppy) + π(NCS)	
52b	−5.9226	1.1	84.2	14.7	π(ppy) + π(NCS)	
52a	−6.1425	17.7	60.7	21.6	d(Ir) + π(ppy) + π(NCS)	15.0 d_{z^2}

posed of 34.0% $d_{x^2-y^2}$(Ir), 11.6% d_{xy}(Ir), and 45.9% π(ppy) with little π(CN) composition, HOMO − 1 and HOMO − 2 with close orbital energy are all dominantly composed of d(Ir) and π(ppy), but with different composition of d(Ir) in detail. MO 51b has 41.1% d_{yz}(Ir) and 9.5% d_{xz}(Ir), while MO 51a is composed of 25.6% d_{xy}(Ir) and 32.4% d_{z^2}(Ir). With respect to **2** and **3**, the first three high energy occupied orbitals are contributed by three units Ir, ppy, and X, in addition, the compositions of X ligand are dramatically larger than **1** because the π electron accepting-ability of NCS and NCO are greater than that of CN. The similar Ru complexes [Ru(4,4′-COOH-2,2′-bpy)$_2$(NCS)$_2$] investigated by Fantacci et al. have different HOMOs components from our Ir complexes, they are dominantly composed of NCS ligand and Ru atom [32]. The Ir component in HOMO and HOMO − 1 of **2** and **3** have the similar component to these of **1**, but the Ir component in HOMO − 2 of **2** and **3** are purely contributed by d_{z^2}(Ir), which is different from that of **1** mixed by d_{z^2}(Ir) and d_{xy}(Ir) orbitals. The differences of the high occupied MOs between **1** and **2**, **3** result from the different π electron-accepting abilities of the X ligands. In addition, Fig. 3 shows that the energy levels of HOMO are changed more significantly than those of LUMO by tuning X ligands.

3.3. The spectroscopic properties in CH_2Cl_2 media

3.3.1. Absorptions

The calculated absorptions (singlet to singlet) in the UV–Vis region simulated in CH_2Cl_2 associated with their oscillator strengths, the main configurations, and the assignments as well as the experimental results are given in Table 5. The fitted Gaussian type absorption curves with the calculated absorption data are displayed in Fig. 2 to show the red-shift effect of the absorptions. To intuitively understand the transition process, the molecular orbital energy levels involved in absorption transitions of **1**–**3** are shown in Fig. 3.

Fig. 2 shows that the lowest-lying distinguishable absorption bands of **1**, **2**, and **3** at 370–420 nm (3.35–2.95 eV), 420–470 nm (2.95–2.64 eV), and 450–500 nm (2.76–2.48 eV), respectively. With respect to **1**, Table 5 shows that the excitation of MO 52a → MO 52b with the configuration coefficient of 0.68905 is in charge of the absorption band at

Table 4
Molecular orbital compositions (%) in the ground state for Ir(ppy)$_2$(NCO)$_2$ (**3**) at B3LYP level

Orbital	Energy (eV)	MO composition			Main bond type	Ir component
		Ir	ppy	NCO		
57a	−1.1840	4.3	94.6	1.1	π*(ppy)	
56b	−1.2468	2.7	96.1	1.2	π*(ppy)	
HOMO–LUMO energy gap						
56a	−4.6208	52.2	30.2	17.6	d(Ir) + π(ppy) + π(NCO)	36.0 $d_{x^2-y^2}$, 14.1 d_{xy}
55b	−5.2263	55.2	19.4	25.4	d(Ir) + π(ppy) + π(NCO)	20.4 d_{yz}, 34.4 d_{xz}
55a	−5.2472	56.3	16.8	26.9	d(Ir) + π(ppy) + π(NCO)	53.7 d_{z^2}
54b	−5.7036	0.9	78.4	20.7	π(ppy) + π(NCO)	
54a	−5.9583	2.3	69.3	28.4	π(ppy) + π(NCO)	
53b	−6.0516	1.0	31.8	67.2	π(ppy) + π(NCO)	

Table 5
Absorptions of **1**–**3** calculated with the TDDFT method, together with the experimental values

	Transition	Config. (CI coeff.)	*E*/nm (eV)	Oscillator	Assignt	$\lambda_{expt.}$/nm (eV)[a]
Singlet → singlet						
1	$X^1A \rightarrow A^1B$	52a → 52b (0.68905)	403 (3.07)	0.0456	MLCT/ILCT	463 (2.68)
	$X^1A \rightarrow B^1B$	51b → 53a (0.49047)	335 (3.71)	0.1725	MLCT/ILCT	
		51a → 52b (0.44842)			MLCT/ILCT	
	$X^1A \rightarrow C^1B$	50b → 54a (0.41002)	275 (4.50)	0.4208	ILCT/MLCT	
2	$X^1A \rightarrow A^1B$	55a → 55b (0.69073)	449 (2.76)	0.0312	MLCT/LLCT/ILCT	476 (2.61)
	$X^1A \rightarrow B^1B$	54b → 56a (0.49439)	369 (3.36)	0.1120	MLCT/LLCT	
		54a → 55b (0.42879)			MLCT/LLCT	
	$X^1A \rightarrow C^1B$	52b → 56a (0.61906)	307 (4.04)	0.1488	LLCT/ILCT	
	$X^1A \rightarrow D^1B$	52a → 56b (0.44466)	264 (4.70)	0.4358	LLCT/ILCT	
3	$X^1A \rightarrow A^1B$	56a → 56b (0.68975)	475 (2.61)	0.0289	MLCT/LLCT/ILCT	497 (2.49)
	$X^1A \rightarrow B^1B$	55b → 57a (0.48683)	375 (3.30)	0.1553	MLCT/LLCT	
		55a → 56b (0.47673)				
	$X^1A \rightarrow C^1B$	54b → 57a (0.62221)	313 (3.96)	0.1585	LLCT/ILCT	
	$X^1A \rightarrow D^1B$	53b → 57a (0.56747)	290 (4.28)	0.1463	LLCT/ILCT	

[a] From Ref. [17].

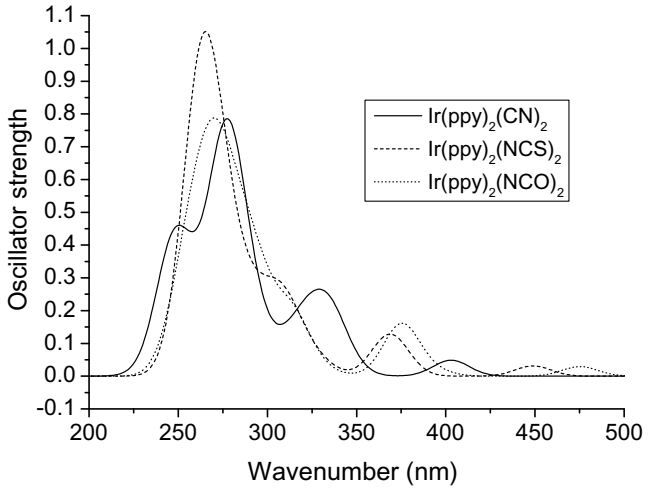

Fig. 2. Simulated absorption spectra of **1**–**3** in CH_2Cl_2 media with the calculated data at TD-B3LYP/LANL2DZ level.

403 nm. Table 2 shows that MO 52a is composed of 34.0% $d_{x^2-y^2}$(Ir), 11.6% d_{xy}(Ir), and 45.9% π(ppy) with little π(CN) composition, while MO 52b is dominantly localized on ppy ligand, thus, this absorption band can be assigned to $\{[d_{x^2-y^2}(\mathrm{Ir}) + d_{xy}(\mathrm{Ir}) + \pi(\mathrm{ppy})] \rightarrow [\pi^*(\mathrm{ppy})]\}$ transition with MLCT and intraligand charge transfer (ILCT) transition characters. But the lowest-lying absorption bands of **2** and **3** at 449 and 475 nm, respectively, have different transition nature. Table 5 shows that the excitations of MO 55a → MO 55b (CI = 0.69073) and MO 56a → MO 56b (CI = 0.68975) should be responsible for these absorptions. According to the discussion on the frontier molecular orbitals, the HOMOs of **2** and **3** have similar d_{z^2}(Ir) and d_{xy}(Ir) compositions to that of **1**, but the NCS and NCO ligands have ca. 20% compositions (see Tables 3 and 4). Thus, these two absorptions are dominantly attributed to $\{[d_{x^2-y^2}(\mathrm{Ir}) + d_{xy}(\mathrm{Ir}) + \pi(\mathrm{ppy}) + \pi(\mathrm{NCS/NCO})] \rightarrow [\pi^*(\mathrm{ppy})]\}$ transition with MLCT/ILCT and ligand-to-ligand charge transfer (LLCT) transition characters. Fig. 2 shows that the lowest-lying absorption of **1**, **2**, and **3** are red-shifted in order **1** < **2** < **3**, which is consistent with the π electron-accepting abilities order **1** < **2** < **3**. The calculated results showed that the transition character can be changed by tuning X ligand, and the excitation energy can be reduced by increasing the π electron-accepting abilities of X ligand.

Fig. 2 show that the second calculated absorptions of **1**, **2**, and **3** are at 335 nm (3.71 eV), 369 nm (3.36 eV), and 375 nm (3.30 eV), respectively, and Table 5 shows that they are dominantly contributed by two excitations with similar CI coefficient. For **1**, the excitations of MO 51b → MO 53a (CI = 0.49047) and MO 51a → MO 52b (CI = 0.44842) are responsible for the absorption at 335 nm. Table 2 shows that MO 51b, lying −5.6521 eV, is contributed by 41.1% d_{yz}(Ir), 9.5% d_{xz}(Ir), and 42.3% π(ppy), while MO 51a, lying −5.6728 eV, has 25.6% d_{xy}(Ir), 32.4% d_{z^2}(Ir), and 31.1% π(ppy). The unoccupied orbitals 53a and 52b are dominantly localized on ppy ligand. Thus, the absorption of **1** at 335 nm can be described as $\{[d_{xz}(\mathrm{Ir}) + d_{yz}(\mathrm{Ir}) + d\text{-}_{z^2}(\mathrm{Ir}) + d_{xy}(\mathrm{Ir}) + \pi(\mathrm{ppy})] \rightarrow [\pi^*(\mathrm{ppy})]\}$ transition with MLCT/ILCT transition characters. The absorption of **2** at 369 nm is contributed by MO 54b → MO 56a (CI = 0.49439) and MO 54a → MO 55b (CI = 0.42879) excitations. Table 3 shows that MO 54b has 13.7% d_{yz}(Ir), 24.9% d_{xz}(Ir), 13.2% π(ppy), and 48.2% π(NCS), while MO 54a is composed of 35.4% d_{z^2}(Ir), 11.3% π(ppy), and 51.8% π(NCS), the unoccupied orbitals 56a and 55b are dominantly contributed by π*(ppy). Thus, the absorption of **2** at 369 nm can be described as $\{[d_{xz}(\mathrm{Ir}) + d_{yz}(\mathrm{Ir}) + d_{z^2}(\mathrm{Ir}) + \pi(\mathrm{ppy}) + \pi(\mathrm{NCS})] \rightarrow [\pi^*(\mathrm{ppy})]\}$ transition with

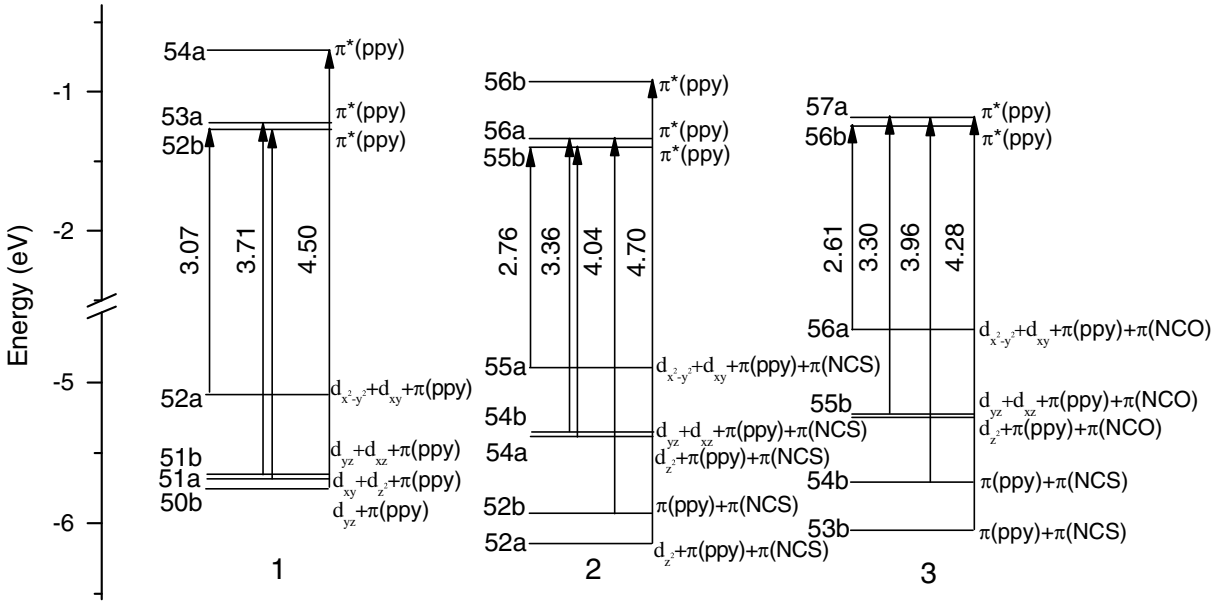

Fig. 3. Diagrams of the molecular orbitals related to the absorptions for **1**–**3** at TD-B3LYP/LANL2DZ level.

Table 6
Phosphorescent emissions of **1**–**3** calculated with TDDFT method, together with the corresponding experimental values

	Transition	Config. (CI Coeff.)	*E*/nm (eV)	Assignt	Exptl./nm (eV)[a]
1	$A^3B \rightarrow X^1A$	52b → 52a (0.57153)	466 (2.66)	^{3}MLCT/^{3}ILCT	470 (2.64)
2	$A^3B \rightarrow X^1A$	55b → 55a (0.61809)	487 (2.55)	^{3}MLCT/^{3}ILCT/^{3}LLCT	506 (2.45)
3	$A^3B \rightarrow X^1A$	56b → 56a (0.67490)	516 (2.40)	^{3}MLCT/^{3}ILCT/^{3}LLCT	538 (2.30)

[a] From Ref. [17].

MLCT/LLCT and ILCT transition characters. The absorption of **3** at 375 nm has similar transition character as that of **2** at 369 nm.

Table 5 shows that the unique absorption bands of **2** and **3** at 307 nm (4.04 eV) and 313 nm (3.96 eV) are contributed by MO 52b → MO 56a (CI = 0.61906) and MO 54b → MO 57a (CI = 0.62221) excitations, respectively. Table 3 shows that MO 52b is composed of 84.2% π(ppy) and 14.7% π(NCS), while MO 56a is dominantly localized on ppy lignad. Thus, the absorption of **2** at 307 nm is attributed to {[π(NCS) + π(ppy)] → [π*(ppy)]} transition with LLCT/ILCT transition characters. Similarly, the absorption of **3** at 313 nm is assigned to {[π(NCO) + π(ppy)] → [π*(ppy)]} transition.

Table 5 and Fig. 2 show that the absorption bands of **1**, **2**, and **3** with the highest excitation energy above 4.0 eV at 275, 264, and 290 nm are contributed by MO 50b → MO 54a (CI = 0.41002), MO 52a → MO 56b (CI = 0.44466), and MO 53b → MO 57a (CI = 0.56747) excitations, respectively. Tables 2–4 shows that MOs 54a, 56b, and 57a are all localized on ppy ligand, MO 50b of **1** has 15.8 d(Ir), and 76.2% π(ppy), MO 52a of **2** is composed by 17.7% d(Ir), 60.7% π(ppy), and 21.6% π(NCS), and MO 53b of **3** is contributed by 31.8% π(ppy) and 67.2% π(NCO). Thus, these high energy absorptions are dominantly assigned to ILCT transition character mixed with other transition character such as MLCT for **1** and **2**, LLCT for **2** and **3**.

Experimentally, the lowest-lying absorptions at 463 nm (2.68 eV), 476 nm (2.61 eV), and 497 nm (2.49 eV) of **1**–**3**, respectively, are all assigned to MLCT transition, and the absorptions of **2** and **3** are red-shifted compared with that of **1**. Furthermore, our calculated absorption bands of **1** (403 nm), **2** (449 nm), and **3** (475 nm) are consistent with the measured excitation energy values and the transition assignments [20].

3.3.2. Phosphorescence

The calculated phosphorescence of **1**–**3** in CH_2Cl_2 media together with the corresponding measured results [20] are given in Table 6; the frontier molecular orbital compositions responsible for the emissions are summarized in Table 7.

The calculated phosphorescence of **1**, **2** and **3** at 466 nm (2.66 eV), 487 nm (2.55 eV), and 516 nm (2.40 eV), respectively, are consistent well with their experimental values [20] at 470 nm (2.64 eV), 506 nm (2.45 eV), and 538 nm (2.30 eV). With respect to **1**, the excitation of MO 52b → MO 52a with the configuration coefficient of 0.57153 is dominantly in charge of the emission at 466 nm. Table 7 shows that MO 52b is a π*(ppy) type orbital with about 97.7% composition, while MO 52a is composed of 35.5% $d_{x^2-y^2}$(Ir), 13.5% d_{xy}(Ir), and 43.7% π(ppy). Thus the emission at 466 nm of **1** can be described as originating from ^{3}\{[$d_{x^2-y^2}$(Ir) + d_{xy}(Ir) + π(ppy)] [π*(ppy)]\} excited state with ^{3}MLCT/^{3}ILCT character. But the emissions at 487 and 516 nm of **2** and **3** have different transition characters. Table 6 shows that the excitation of MO 55b → MO 55a (CI = 0.61809) causes the emission of **2** at 487 nm. Table 7 shows that MO 55b has similar composition as MO 52b of **1**, while the MO 55a has 32.8% $d_{x^2-y^2}$(Ir), 12.5% d_{xy}(Ir), 27.7% π(ppy), and 25.4%

Table 7
Molecular orbital compositions (%) in the A^3B excited states for $Ir(ppy)_2(CN)_2$ (**1**), $Ir(ppy)_2(NCS)_2$ (**2**), and $Ir(ppy)_2(NCO)_2$ (**3**) at B3LYP/LANL2DZ level

Orbital	Energy (eV)	MO composition			Main bond type	Ir component
		Ir	ppy	X		
1						
52b	−1.2697	1.4	97.7	0.9	π*(ppy)	
52a	−5.0331	50.4	43.7	5.9	d(Ir) + π(ppy)	35.5 $d_{x^2-y^2}$, 13.5 d_{xy}
2						
55b	−1.4123	1.7	97.1	1.2	π*(ppy)	
55a	−4.9103	46.9	27.7	25.4	d(Ir) + π(ppy) + π(NCS)	32.8 $d_{x^2-y^2}$, 12.5 d_{xy}
3						
56b	−1.2574	1.8	97.3	0.9	π*(ppy)	
56a	−4.5901	54.0	27.1	18.9	d(Ir) + π(ppy) + π(NCO)	37.3 $d_{x^2-y^2}$, 14.6 d_{xy}

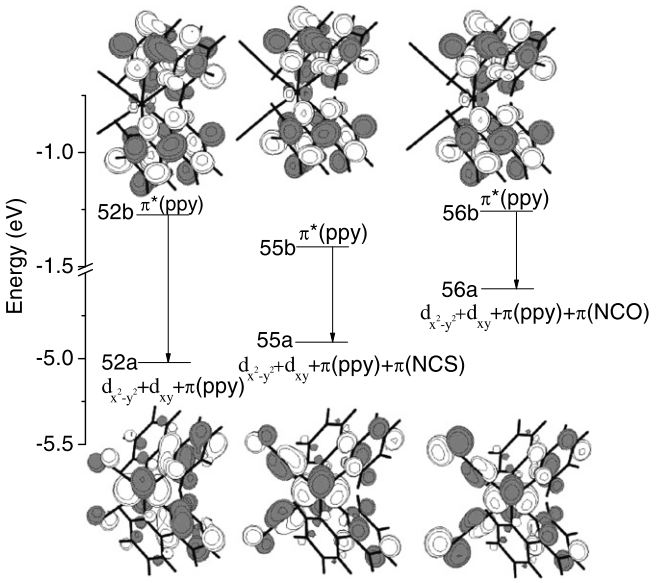

Fig. 4. Transitions contributing to the emissions at 466, 487, and 516 nm for **1**–**3**, respectively, simulated in CH_2Cl_2 media at TD-B3LYP/LANL2DZ level.

π(NCS). Thus, the emission of **2** at 487 nm can be described as originating from $^3\{[d_{x^2-y^2}(Ir)+d_{xy}(Ir)+\pi(ppy)+\pi(NCS)][\pi^*(ppy)]\}$ excited state with ^{3}MLCT/^{3}ILCT/^{3}LLCT character. The nature of the phosphorescence of **3** at 516 nm is similar to that of **2** at 487 nm (see Table 7). Compared **1** with **2** and **3**, the emission results indicated that ligand X can participate in the emission transition when the π electron-accepting ability of ligand X is increased, which results in the red-shift of the emission spectra of **2** and **3**. Fig. 4 displays intuitive electron transition diagrams of the emission. Experimentally, the measured phosphorescence in CH_2Cl_2 media of **1**, **2**, and **3** at 470 nm (2.64 eV), 506 nm (2.45 eV), and 538 nm (2.30 eV), respectively, are all tentatively assigned to a ^{3}MLCT and $^3\pi$–π^* emission, which is consistent with our calculated assignments [20].

The discussions on absorptions reveal that the calculated lowest-lying absorption of **1** at 403 nm dominantly arises from the combination of MLCT and ILCT transitions and those of **2** and **3** at 449 and 475 nm are assigned to MLCT/ILCT/LLCT transition, thus the calculated phosphorescence is just the reverse process of the lowest-lying absorption because of the same transition character and symmetry. The energy differences between the calculated lowest-lying absorption and the phosphorescence of **1**, **2**, and **3** are 0.41 eV, 0.21 eV, and 0.21 eV, respectively.

In previous investigations, many researchers have concluded that there is a competition between the MLCT and $[\pi \rightarrow \pi^*]$ ligand-centered (LC) transitions due to the very close energy levels of the terminal orbitals of the complexes [34]. According to our present studies, the calculated combined MLCT/ILCT transition natures of the absorptions in the UV–Vis region have confirmed previous prediction. Furthermore, now we note that by increasing the π electron-accepting ability of X ligand, the HOMO of **2** and **3** have greater X compositions than that of **1**, which is different from the previous studies that X ligand had little composition of HOMO, thus, the X ligand can participate in the absorption and emission transitions. Therefore, the calculated results indicated that there is an LLCT type excitation transition in the competition between MLCT and ILCT type transitions, and one of the decisive factors is the π electron-accepting ability of X ligands.

Obviously, both of the calculated and the experimental results showed that the phosphorescence can be tuned by changing the π electron-accepting abilities of X ligands [20] besides by changing the C^N ligands according to previously experimental investigations [11]. The X ligands with stronger π electron-accepting ability will lead to more red-shifts in the absorption and emission spectra.

4. Conclusions

The present work investigated the ground and excited state geometries, absorption, and phosphorescence of three bis-cyclometalated iridium(III) complexes with ppy, CN, NCS, and NCO ligands theoretically. The calculated results revealed that HOMO can be significantly changed by tuning X ligands, but LUMO is hardly affected. The lowest-lying absorption at 403 nm of **1** is assigned to MLCT/ILCT transition, while those of **2** and **3** at 449 and 475 nm can be described as MLCT/ILCT/LLCT transitions. The phosphorescence of **1** at 466 nm originates from ^{3}MLCT/^{3}ILCT excited state, while those of **2** and **3** at 487 and 516 nm are from ^{3}MLCT/^{3}ILCT/^{3}LLCT excited states. The calculated results showed that the emission colors can be tuned by changing π electron-accepting ability of X ligand, and the ligand X can participate in the absorption and emission transition processes. So it is very practical to explore the relationship between X ligand and phosphorescent properties of bis-cyclometalated iridium(III) complexes. We hope these theoretical studies can provide suggestion in designing highly efficient phosphorescent materials.

Acknowledgement

This work was supported by the Natural Science Foundation of China (Grant Nos. 20173021, 20333050, and 20573042).

References

[1] (a) V. Balzani, A. Juris, M. Venturi, S. Campagna, S. Serroni, Chem. Rev. 96 (1996) 759;
(b) J.N. Demas, B.A. DeGraff, Coord. Chem. Rev. 211 (2001) 317.
[2] (a) Md.K. Nazeeruddin, R.T. Wegh, Z. Zhou, C. Klein, Q. Wang, F. De Angelis, S. Fantacci, M. Gratzel, Inorg. Chem. 45 (2006) 9245;
(b) F. De Angelis, S. Fantacci, A. Selloni, Chem. Phys. Lett 289 (2004) 204.

[3] K.D. Demadis, C.M. Hartshorn, T.J. Meyer, Chem. Rev. 101 (2001) 2655.
[4] (a) K.M. Cheung, Q.F. Zhang, K.W. Chan, M.H.W. Lam, I.D. Williams, W.H. Leung, J. Organomet. Chem. 690 (2005) 2913;
(b) M.K. Lau, K.M. Cheung, Q.F. Zhang, Y.L. Song, W.T. Wong, I.D. Williams, W.H. Leung, J. Organomet. Chem. 689 (2004) 2401.
[5] (a) Y. Wand, N. Herron, V.V. Grushin, D.D. LeCloux, V.A. Petrov, Appl. Phys. Lett. 79 (2001) 449;
(b) H. Xin, F.Y. Li, M. Shi, Z.Q. Bian, H.Ch. Huang, J. Am. Chem. Soc. 125 (2003) 7166;
(c) A. Tsuboyama, H. Iwawaki, M. Furugori, T. Mukaide, J. Kamatani, S. Igawa, T. Moriyama, S. Miura, T. Takiguchi, S. Okada, M. Hoshino, K. Ueno, J. Am. Chem. Soc. 125 (2003) 12971;
(d) L. Flamigni, B. Ventura, F. Barigelletti, E. Baranoff, J.-P. Collin, J.-P. Sauvage, Eur. J. Inorg. Chem. (2005) 1312;
(e) R.J. Holmes, S.R. Forrest, Y.J. Tung, R.C. Kwong, J.J. Brown, S. Garon, M.E. Thompson, Appl. Phys. Lett. 82 (2003) 2422.
[6] (a) K.K.W. Lo, C.K. Chung, T.K.M. Lee, L.H. Lui, K.H.K. Tsang, N.Y. Zhu, Inorg. Chem. 42 (2003) 6886;
(b) K.K.W. Lo, D.C.M. Ng, C.K. Chung, Organometallics 20 (2001) 4999.
[7] (a) N.D. Silaware, A.S. Goldman, R. Ritter, D.R. Tyler, Inorg. Chem. 28 (1989) 1231;
(b) K.A. Belmore, R.A. Vanderpool, J.C. Tsai, M.A. Khan, K.M. Nicholas, J. Am. Chem. Soc. 110 (1988) 2004.
[8] (a) M.C. DeRosa, D.J. Hodgson, G.D. Enright, B. Dawson, C.E.B. Evans, R.J. Crutchley, J. Am. Chem. Soc. 126 (2004) 7619;
(b) G. Di Marco, M. Lanza, A. Mamo, I. Stefio, C. Di Pietro, G. Romeo, S. Campagna, Anal. Chem. 70 (1998) 5019;
(c) M.L. Ho, F.M. Hwang, P.N. Chen, Y.H. Hu, Y.M. Cheng, K.S. Chen, G.H. Lee, Y. Chi, P.T. Chou, Org. Biomol. Chem. 4 (2006) 98;
(d) M.A. Nolan, S.P. Kounaves, Anal. Chem. 71 (1999) 3567;
(e) Q. Zhao, T.Y. Cao, F.Y. Li, X.H. Li, H. Jing, T. Yi, C.H. Huang, Organometallics 26 (2007) 2077.
[9] C. Adachi, M.A. Baldo, S.R. Forrest, M.E. Thompson, Appl. Phys. Lett. 77 (2000) 904.
[10] (a) W.Y. Wong, G.J. Zhou, X.M. Yu, H.S. Kwok, Z.Y. Lin, Adv. Funct. Mater. 17 (2007) 315;
(b) W.Y. Wong, C.L. Ho, Z.Q. Gao, B.X. Mi, C.H. Chen, K.W. Cheah, Z.Y. Lin, Angew. Chem. Int. Ed. 45 (2006) 7800;
(c) X.M. Yu, H.S. Kwok, W.Y. Wong, G.J. Zhou, Chem. Mater. 18 (2006) 5097;
(d) G.J. Zhou, W.Y. Wong, B. Yao, Z.Y. Xie, L.X. Wang, Angew. Chem. Int. Ed. 46 (2007) 1149;
(e) L. Liu, S.Y. Poon, W.Y. Wong, J. Organomet. Chem. 690 (2005) 5036;
(f) W.Y. Wong, G.J. Zhou, X.M. Yu, H.S. Kwok, B.Z. Tang, Adv. Funct. Mater. 16 (2006) 838.
[11] (a) S. Lamansky, P. Djurovich, D. Murphy, F. Abdel-Razzaq, H.E. Lee, C. Adachi, P.E. Burrows, S.R. Forrest, M.E. Thompson, J. Am. Chem. Soc. 123 (2001) 4304;
(b) S. Lamansky, P. Djurovich, D. Murphy, F. Abdel-Razzaq, R. Kwong, I. Tsyba, M. Bortz, B. Mui, R. Bau, M.E. Thompson, Inorg. Chem. 40 (2001) 1704.
[12] (a) M. Lepeltier, T.K.-M. Lee, K.K.-W. Lo, L. Toupet, H.L. Bozec, V. Guerchais, Eur. J. Inorg. Chem. (2007) 2734;
(b) K.K.-W. Lo, J.S.-Y. Lau, D.K.-K. Lo, L.T.-L. Lo, Eur. J. Inorg. Chem. (2006) 4054;
(c) K. Ono, M. Joho, K. Saito, M. Tomura, Y. Matsushita, S. Naka, H. Okada, H. Onnagawa, Eur. J. Inorg. Chem. (2006) 3676;
(d) C.S. Chin, M.-S. Eum, S.y. Kim, C. Kim, S.K. Kang, Eur. J. Inorg. Chem. (2006) 4979.
[13] P.J. Hay, J. Phys. Chem. A 106 (2002) 1634.
[14] (a) J.P.J. Markham, S.-C. Lo, S.W. Magennis, P.L. Burn, I.D.W. Samuel, Appl. Phys. Lett. 80 (2002) 2645;
(b) C. Adachi, M.A. Baldo, S.R. Forrest, Appl. Phys. Lett. 77 (2000) 904;
(c) M.G. Colombo, H.U. Gudel, Inorg. Chem. 32 (1993) 3081;
(d) M.A. Baldo, S. Lamansky, P.E. Burrows, M.E. Thompson, S.R. Forrest, Appl. Phys. Lett. 75 (1999) 4;
(e) J.C. Ostrowski, M.R. Robinson, A.J. Heeger, G.C. Bazan, Chem. Commun. (2002) 784;
(f) K.A. King, P.J. Spellane, R.J. Watts, J. Am. Chem. Soc. 107 (1985) 1431;
(g) C.J. Chang, C.H. Yang, K. Chen, Y. Chi, C.F. Shu, M.L. Ho, Y.S. Yeh, P.T. Chou, Dalton Trans. (2007) 1881.
[15] A.B. Tamayo, B.D. Alleyne, P.I. Djurovich, S. Lamansky, I. Tsyba, N.N. Ho, R. Bau, M.E. Thompson, J. Am. Chem. Soc. 125 (2003) 7377.
[16] (a) R.J. Holmes, B.W. D'Andrade, S.R. Forrest, X. Ren, J. Li, M.E. Thompson, Appl. Phys. Lett. 83 (2003) 3818;
(b) T. Sajoto, P.I. Djurovich, A. Tamayo, M. Yousufuddin, R. Bau, M.E. Thompson, R.J. Holmes, S.R. Forrest, Inorg. Chem. 44 (2005) 7992;
(c) A.B. Tamayo, S. Garon, T. Sajoto, P.I. Djurovich, I.M. Tsyba, R. Bau, M.E. Thompson, Inorg. Chem. 44 (2005) 8723;
(d) R.J. Holmes, S.R. Forrest, T. Sajoto, A. Tamayo, P.I. Djurovich, M.E. Thompson, J. Brooks, Y.-J. Tung, B.W. D'Andrade, M.S. Weaver, R.C. Kwong, J.J. Brown, Appl. Phys. Lett. (2005) 243507.
[17] (a) N. Yoshikawa, S. Yamabe, N. Kanehisa, Y. Kai, H. Takashima, K. Tsukahara, Eur. J. Inorg. Chem. (2007) 1911;
(b) T.H. Kwon, H.S. Cho, M.K. Kim, J.W. Kim, J.J. Kim, K.H. Lee, S.J. Park, I.S. Shin, H. Kim, D.M. Shin, Y.K. Chung, J.I. Hong, Organometallics 24 (2005) 1578;
(c) Q. Zhao, S.J. Liu, M. Shi, C.M. Wang, M.X. Yu, L. Li, F.Y. Li, T. Yi, C.H. Huang, Inorg. Chem. 45 (2006) 6152.
[18] (a) Y.S. Kim, H.L. Young, Curr. Appl. Phys. 7 (2007) 504;
(b) Y.S. Kim, H.L. Young, Thin Solid Films 515 (2007) 5079.
[19] (a) T. Liu, H.X. Zhang, X. Shu, B.H. Xia, Dalton Trans. (2007) 1922;
(b) T. Liu, B.H. Xia, X. Zhou, H.X. Zhang, Q.J. Pan, J.S. Gao, Organometallics 26 (2007) 143;
(c) T. Liu, H.X. Zhang, B.H. Xia, J. Phys. Chem. A 111 (2007) 8724;
(d) X. Zhou, H.X. Zhang, Q.J. Pan, M.X. Li, Y. Wang, C.M. Che, Eur. J. Inorg. Chem. (2007) 2181;
(e) M.X. Li, H.X. Zhang, X. Zhou, Q.J. Pan, H.G. Fu, C.C. Sun, Eur. J. Inorg. Chem. (2007) 2171.
[20] Md.K. Nazeeruddin, R. Humphry-Baker, D. Berner, S. Rivier, L. Zuppiroli, M. Graetzel, J. Am. Chem. Soc. 125 (2003) 8790.
[21] E. Runge, E.K.U. Gross, Phys. Rev. Lett. 52 (1984) 997.
[22] A.D. Becke, J. Chem. Phys. 98 (1993) 5648.
[23] (a) R.E. Stratmann, G.E. Scuseria, J. Chem. Phys. 109 (1998) 8218;
(b) N.N. Matsuzawa, A. Ishitani, J. Phys. Chem. A 105 (2001) 4953;
(c) M.E. Casida, C. Jamorski, K.C. Casida, D.R. Salahub, J. Chem. Phys. 108 (1998) 4439.
[24] (a) M. Cossi, G. Scalmani, N. Regar, V. Barone, J. Chem. Phys. 117 (2002) 43;
(b) V. Barone, M. Cossi, J. Chem. Phys. 107 (1997) 3210.
[25] K. Raghavachari, J.A. Pople, Int. J. Quantum Chem. 20 (1981) 1067.
[26] M.D. Halls, H.B. Schlegel, Chem. Mater. 13 (2001) 2632.
[27] (a) X. Zhou, A.-M. Ren, J.-K. Feng, Polymer 45 (2004) 7747;
(b) J.-F. Wang, J.-K. Feng, Macromolecules 37 (2004) 3451;
(c) L. Yang, A.-M. Ren, J.-K. Feng, J.-F. Wang, J. Org. Chem. 70 (2005) 3009.
[28] J.B. Foresman, M. Head-Gordon, J.A. Pople, M.J. Frisch, J. Phys. Chem. 96 (1992) 135.
[29] M.E. Casida, C. Jamorski, K.C. Casida, D.R. Salahub, J. Chem. Phys. 108 (1998) 4439.
[30] (a) P.J. Hay, W.R. Wadt, J. Chem. Phys. 82 (1985) 299;
(b) P.J. Hay, W.R. Wadt, J. Chem. Phys. 82 (1985) 270.
[31] M.J. Frisch, G.W. Trucks, H.B. Schlegel, G.E. Scuseria, M.A. Robb, J.R. Cheeseman, J.A. Montgomery Jr., T. Vreven, K.N. Kudin, J.C. Burant, J.M. Millam, S.S. Iyengar, J. Tomasi, V. Barone, B. Mennucci, M. Cossi, G. Scalmani, N. Rega, G.A. Petersson, H Nakatsuji,. M.

Hada, M. Ehara, K. Toyota, R. Fukuda, J. Hasegawa, M. Ishida, T. Nakajima, Y. Honda, O. Kitao, H. Nakai, M. Klene, X. Li, J.E. Knox, H.P. Hratchian, J.B. Cross, C. Adamo, J. Jaramillo, R. Gomperts, R.E. Stratmann, O. Yazyev, A.J. Austin, R. Cammi, C. Pomelli, J.W. Ochterski, P.Y. Ayala, K. Morokuma, G.A. Voth, P. Salvador, J.J. Dannenberg, V.G. Zakrzewski, S. Dapprich, A.D. Daniels, M.C. Strain, O. Farkas, D.K. Malick, A.D. Rabuck, K. Raghavachari, J.B. Foresman, J.V. Ortiz, Q. Cui, A.G. Baboul, S. Clifford, J. Cioslowski, B.B. Stefanov, G. Liu, A. Liashenko, P. Piskorz, I. Komaromi, R.L. Martin, D.J Fox,. T. Keith, M.A. Al-Laham, C.Y. Peng, A. Nanayakkara, M. Challacombe, P.M.W. Gill, B. Johnson, W. Chen, M.W. Wong, C. Gonzalez, J.A. Pople, GAUSSIAN 03, Revision C.02, Gaussian, Inc., Wallingford, CT, 2004.

[32] S. Fantacci, F.D. Angelis, A. Selloni, J. Am. Chem. Soc. 125 (2003) 4381.

[33] Y.H. Zhang, B.H. Xia, Q.J. Pan, H.X. Zhang, J. Chem. Phys. 124 (2006) 144309.

[34] (a) M. Feliz, G. Ferraudi, Inorg. Chem. 37 (1998) 2806;
(b) N. Chanda, B. Sarkar, S. Kar, J. Fiedler, W. Kaim, G.K. Lahiri, Inorg. Chem. 43 (2004) 5128;
(c) J.D. Lewis, R.N. Perutz, J.N. Moore, J. Phys. Chem. A 108 (2004) 9037.